Perfomance Evaluation Of A Singal Crystal Hydrophone

Paul James Seekings, Teong Beng Koay, Mandar Chitre, Venugopalan Payallil, Parijat Deshpande
Acoustic Research Laboratory, Tropical Marine Science Institute,
National University of Singapore, 12a Kent Ridge Road, Singapore 119223.

Jing Jin, Leong-chew Lim
Materials Technologies P/L.

paul@arl.nus.edu.sg

Abstract - **Relaxor single crystals such as PZN-PT and PMN-PT exhibit superior electromechanical properties and are touted as the next-generation materials for future high performance piezo devices. This work describes a new hydrophone made of high-sensitivity PZN-PT single crystal d_{31} sensing elements. Three such elements are mounted in custom-made housing. A compartment is provided to house the three pre-amplifiers, one for each element. In the current prototype each element has its own input. This allows the directionality of each element to be measured and the possibility of locating the source direction from the combined signals of the three elements. A compact low noise high impedance voltage follower pre-amplifier has been designed which provides 26dB of gain. The overall sensitivity was measured to be -169dB re 1 V/µPa. Directionality has been measured to be approximately omni-directional within ±1dB, up to a frequency of 7 kHz.**

I. INTRODUCTION

Single crystals have very attractive properties compared to conventional piezo composites as sensing element of hydrophones. Due to their higher piezoelectric constants, single crystals give a higher voltage output per unit pressure than piezo composites. This increases the sensitivity of the resultant hydrophone for a given size of sensing elements used.

In this paper, we describe a prototype hydrophone which utilizes single crystal active elements as the acoustic pressure sensors, and low noise front end pre-amplifiers which give good sensitivity in a compact hydrophone unit.

II. FABRICATION OF HIGH-SENSITIVITY SINGLE CRYSTAL HYDROPHONE

The sensitivity of a piezoelectric sensing element can be estimated based on the constitutive equation below:

$$S = sT + dE \quad (1)$$

$$D = \varepsilon E + dT \quad (2)$$

where S is the induced strain, T the applied stress, E the applied electrical field, D the electrical displacement, s the elastic compliance, d the piezoelectric strain coefficient, and ε the dielectric permittivity. The voltage sensitivity, V/p, where V is the voltage output, and p the acoustic pressure, can be obtained from (1) and (2), as follows:

$$V/p = dt/\varepsilon = gt \quad (3)$$

t in (3) is the thickness of the sensing element, and g ($=d/\varepsilon$) is the piezoelectric voltage constant. Note that under near static condition, the sensitivity of an acoustic wave sensor is a product of its piezoelectric voltage constant (g) and thickness (t). Under dynamic conditions, one also needs to take into consideration the acoustic matching, wave transmission and reflection characteristics of the sensing elements.

A. Selection of Single Crystal Sensing Element

High-homogeneity high-performance flux-grown $Pb(Zn_{1/3}Nb_{2/3})O_3$-$PbTiO_3$ (PZN-PT) single crystal produced by *Microfine Materials Technologies P/L* was used in the present project. In order to achieve high voltage sensitivity and to obtain sufficiently high electrical impedance of the resultant sensor, d_{31}-sensing mode PZN-7%PT single crystal active elements were selected. This means that the sensing element used is in the form of a plate, electrically poled in the thickness direction. It senses the acoustic pressure at one of the end faces and generates a corresponding voltage output across the electroded faces. This is shown schematically in Fig. 1.

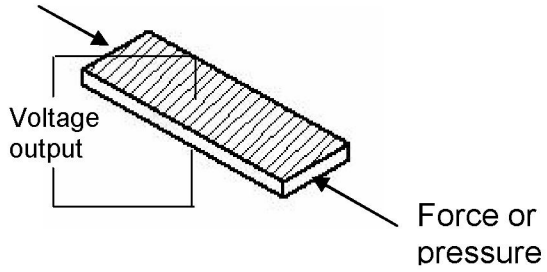

Fig. 1: Schematic of a d_{31} single crystal sensing plate

The single crystal d_{31}-sensing elements are about $12^{L}\times4^{W}\times1.6^{t}$ mm^3 in dimensions. After grinding and polishing to the desired dimensions, the plates were

1-4244-0138-0/06/$20.00 ©2006 IEEE

vacuum coated on both of the largest $L \times w$ faces, first with a thin bondcoat of nichrome and then a layer of gold-palladium electrode. After coating, the plates were optimally poled in the thickness direction in silicone oil at room temperature. The measured properties of the poling crystals are given in TABLE 1. Also given in the table are the properties of state-of-the-art PZT ceramics for comparison purposes. It is evident from this table that PZN7%-PT single crystal d_{31} plates give superior d_{31} and g_{31} values, being more than 5 times in value compared with those of state-of-the-art lead zirconate titanate (PZT) ceramics.

TABLE 1
Transverse properties of high-sensitivity PZN-7%PT single crystal used

Material	d_{31} (pC/N)	k_{31}	K^T	g_{31} (Vm/N)*
PZN-7%PT	3000-4000	>0.9	5000-6000	0.07-0.08
PZT	220	0.5	2000	0.012

*$g_{31} = d_{31} / \varepsilon_{33} = d_{31} / (K^T \varepsilon_o)$; ε_o (permittivity of vacuum) = 8.854×10^{-12} C^2/Nm^2.

B. Modular Design of hydrophone

Fig. 2 shows the modular design of the intended hydrophone. It consists of a waterproof acoustic window hydrophone compartment and the pre-amplifier compartment. The overall dimensions are Ø36mm×48mm, excluding the 2 mm thick waterproof encapsulation.

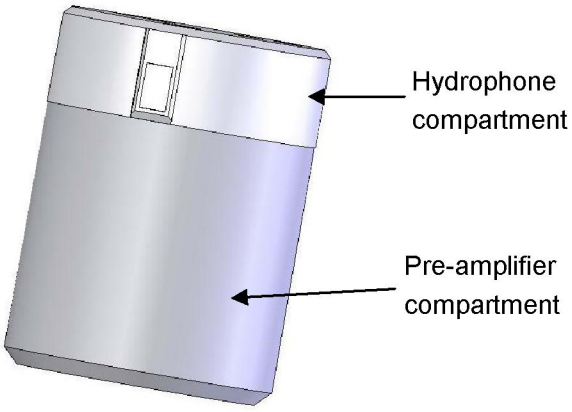

Fig. 2: Module design of vector sensor

C. Construction of individual sensor modules

The modular sensor element design, shown in Fig. 3, is adopted for enhanced robustness and ease of quality control and assembly. Each sensor module is made up of a poled PZN-7%PT single crystal d_{31} plates, of $12^L \times 4^W \times 1.6^T$ mm^3 in dimensions. All poled single crystal plates used registered d_{31} values higher than 3000 pC/N. The $4^W \times 1.6^t$ end of the single crystal plate was used as the sensing area, via interaction with water through the acoustic window of the housing. The single crystal sensing element was first bonded onto a 1 mm thick alumina backing plate by means of epoxy. After curing, the alumina backing plate was bonded onto the base of the module housing with epoxy and carefully inserted into the front end of the module and secured with screws.

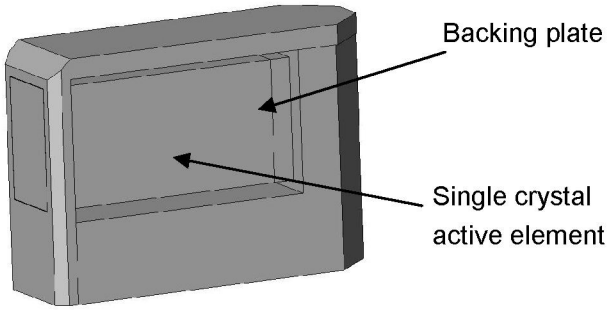

Fig. 3: Individual sensor module

D. Construction of hydrophone compartment

The hydrophone consists of three sensor modules at about 120° apart. Having 3 sensor modules of individual voltage output is advantageous in that this gives:

(a) more even omni-directionality,
(b) enhanced sensitivity (sum of 3 sensor outputs),
(c) improved robustness (i.e. remains functional even if one or two of the sensing elements fail) and
(d) possible estimation of direction of arrival by comparing phase differences between the 3 sensor outputs.

The assembled hydrophone sensor and integrated pre-amps is moulded with 2 mm thick acoustic window material. The fabricated prototype is shown in Fig. 4. Silicon rubber is used as the tentative window material in this prototype, as shown in the picture; polyurethane will be used in the final version.

Fig. 4: Photograph of a single crystal hydrophone prototype

E. Design of Pre-amps

In this prototype version of the hydrophone, each of the three hydrophone elements has an

independent preamp and output. The sensitivity of the hydrophone without pre-amps was found to be -194dBV re 1µPa. In order to meet the design specification, a 25dB pre-amp was designed and built such that the impedance of the sensor is matched at its input and low impedance is presented at its output.

The design of pre-amps is based around a high impedance voltage follower. The operational amplifier was selected with the lowest possible current noise, as this will be the main noise contribution when interfacing with a high impedance source [1,2,3]. Any noise introduced near the sensor will go through the same order of amplification as the sensor signal and therefore should be suppressed efficiently in order to maintain high signal to noise ratio (SNR).

The overall design is such that we provide a base PCB that is to be mechanically mounted to the bottom of hydrophone chassis. The incoming power supply cable and preamplied analog output cables will be soldered into this PCB with enough mechanical strength to minimize contact vibration which will appear in data as signal noise. Three independent and identical analog front end modules will be soldered onto this base PCB.

Apart from providing mechanical support, the base board also regulates the incoming power supply before providing them to the analog front end. The power supply is chosen to be ultra low noise, small size linear regulator. They take ±5.5V~±20V supply and provide ±5V output with ripple noise in micro volts range. This provides the flexibility of using wide input range power supply and minimizes the contamination of power supply noise into signal.The design also provides an option to accommodate single +5V supply input and generate ±5V to the front end modules with minor degrade of the power supply noise performance. For this, a low noise switching DC/DC converter is implemented before the negative supply regulator to generate negative supply from positive voltage.

Two top range high input impedance op amps, LT1169, and LTC6421 were evaluated for their noise and gain-bandwidth performance. Both units have very high input impedance and very low bias current, giving us superior noise performance. For example LT1169 has 6nV/√Hz and 1fA/√Hz while LTC6421 has 7nV/√Hz and 0.6fA/√Hz typically. Both units have low input capacitance of 1.5pF and 3pF with good Gain Bandwidth Product of 5.3MHz and 18MHz. The output offset of LTC6421 is lower than LT1169 (0.2mV compared to 2mV).

Hydrophones are charge emitting transducers. There are two main approaches to translate the input charge variation of and charge-emitting device to an output voltage change: the first is through a charge amplifier and the second is by using a high impedance voltage follower. Charge amplifier has the advantage of being able to accommodate larger variance in capacitance, hence supports long cable. The disadvantage is that its circuitry noise is generally higher than the high impedance voltage follower. The high input impedance follower on the other hand, has the advantage that its noise gain can be controlled easily, thus achieving better noise performance. However, it can be sensitive to any intermittent capacitance limiting it to short cable application. Since the pre-amplifers are located close to sensor, this does not pose as a problem to us. Hence, the high impedance voltage follower is implemented to take advantage of its lower noise characteristics.

LTC6421 is pin compatible to LT1169, hence we use the same circuitry for both. A drawback of the LT1169 was that it presented a relatively high dc offset (up to 2mV); this was unacceptable for the first stage circuitry, as it would have reduced the effective dynamic range. A DC servo was implemented to rectify this issue, making sure that any dc offset would be compensated so that the output voltage would always swing around the signal ground.

Currently the power supply for the circuitry is kept at ±5V although the maximum rating of this device is ±20V. This is done so that the gate-to-junction leakage current is reduced and the heat generation was minimized at the same time. If higher voltage swing is needed, a higher voltage power supply can be used.

Fig. 5 shows the actual analog front end which is partially mounted in the chassis. The base PCB that provides regulated power supply to the preamps is round in shape and fits into the hydrophone chassis. The three analog frond ends are soldered vertically onto the base PCB. We provided good solid ground planes to ensure good noise performance.

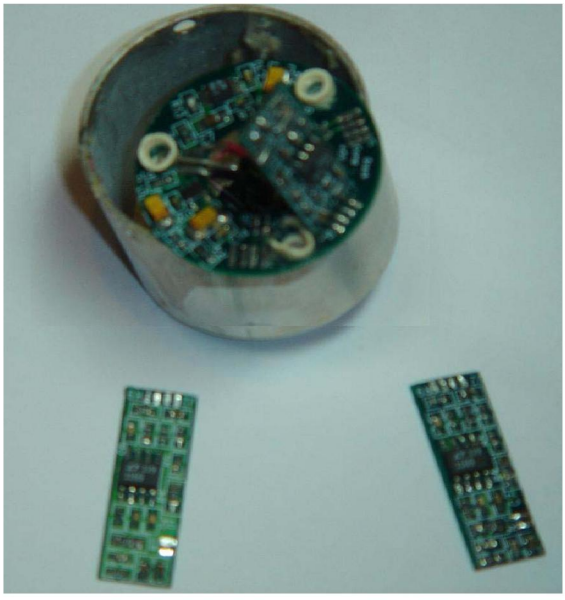

Fig. 5: The Front end analogue and their power supply

III. TESTING OF THE ELECTRONICS

The basic tests done on the preamps are transfer function of the electronics (excluding the sensor transfer function), estimations overall self-noise of

sensor plus electronics, and frequency response of the unit.

The transfer function of the pre-amplifiers are measured using Stanford Research System's signal analyzer model SR785, with the pre-amplifiers' inputs terminated with equivalent impedance of the sensor. A sine sweep is provided from 100Hz to 50 kHz is injected into the Unit under test and the output is observed to realize the frequency response. The experiment schematics and typical transfer function curve of the electronics channels are provided in Fig. 6.

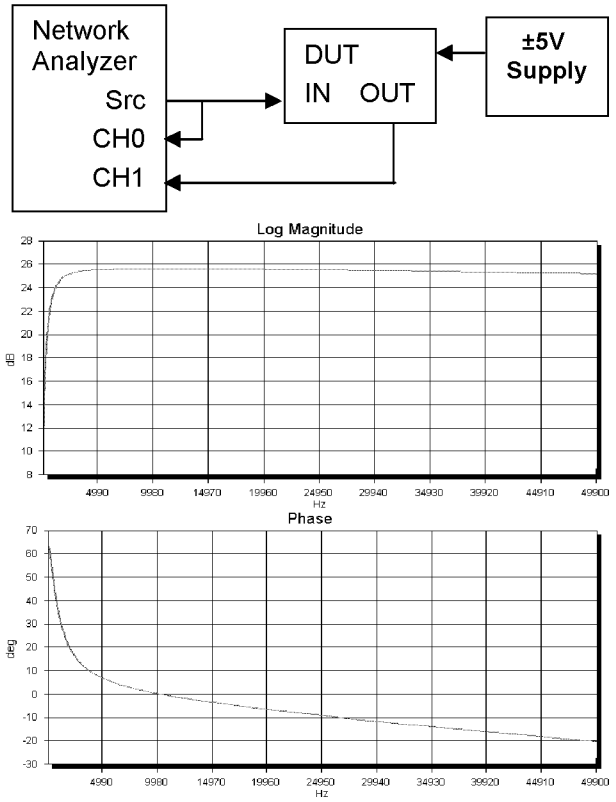

Fig. 6: Analog electronics bench test schematic and typical transfer function

A. *Preliminary estimation of self-noise*

The broadband self-noise of the unit is estimated using Tektronix digital oscilloscope that is setup up to observe 20MHz bandwidth. The fully assembles unit is placed in a foam protection to minimize mechanical vibration and is powered through a HP laboratory power supply as shown in .

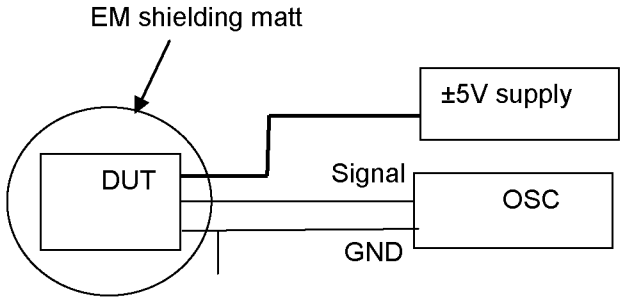

Fig. 7: schematics of self-noise measurement

The noise performance has been evaluated in three setups: the front end itself with equivalent impedence terminated at its input, the front end with single crystal sensor in air and the front end single crystal assembled in the chassis. Each reading is zero meaned before the peak to peak values and r.m.s. values are recorded. Five measurements has been done on each channels at each setup. And the results are shown in TABLE 2.

TABLE 2
Estimated electronics self-noise

Channel	Gain (dB)	Noise Peak-to-peak/r.m.s. (mV)		
		Electronics	Electronics with sensor	Placed in housing
1	25.6	2.4/0.3	2.4/0.3	2.2/0.27
2	25.5	3.2/0.44	3.2/0.47	2.3/0.27
3	25.6	3/0.38	3/0.44	2.4/0.25

Taking the maximum self noise to be 0.27 mV r.m.s,, equivalent self noise expressed in terms of pressure is 54 dB re 1uPa/√Hz assuming the noise bandwidth is limited by the hydrophone operating frequency range of 20kHz. Note that this measurement is done using an oscilloscope set to 20MHz bandwidth without a Faraday cage; therefore the noise measure could include significant out of band contaminations up to 20MHz (up to 30dB more bandwidth). This represents the upper limit of the self noise power and we would expect the actual self-noise to be much smaller.

B. *Evaluation of Sensitivity and directionality*

In order to estimate the sensitivity, we calibrated the hydrophone against a standard CT10 reference, the specification is shown in TABLE 3. The Single crystal hydrophone is mounted on the bottom of a steel pole using a plastic collar. The reference hydrophone was located next to the single crystal hydrophone. A source transducer was used to emit a frequency sweep from a few Hz to 25 kHz. Due to the source transducer used and the limitations of the size of the tank, which affect the amplitude and propagation of lower frequencies, the results are shown starting from 2 kHz up to 20 kHz.

TABLE 3
CT10 Reference hydrophone specification

Receiving sensitivity (re 1μPa/V)	-211dB ±3dB
Frequency range	1Hz ~ 170kHz
Horizontal directivity	±2dB @ 100kHz
Vertical directivity	±3dB @ 100kHz (except near the cab housing)
Nominal capacitance	3.4nF

To minimize the effect of directionality of the reference hydrophone, the standing waves and nulls in the tank, the sweep was repeated while moving the

source transducer around the tank. The power spectrum of the received signals for the CT10 reference and each channel of the single crystal hydrophone are calculated and averaged over the repeated measurements. The top graph of Fig. 8 shows the power spectrum of the received signal on the reference and each of the channels of the single crystal hydrophone without pre-amp. The single crystal element follows the shape of the reference hydrophone, but is around 10 to 12 dB more sensitive.

Fig. 8 also shows the calibration curves of the signal crystal hydrophone without pre-amp. Each element is within 2-3dB of each other, certainly in the design frequency range up to 7kHz. The single crystal hydrophone is 10 to 12 dB better than the reference. Given that sensitivity of the CT10 is -211 dBV re 1 µPa, we can estimate the sensitivity of the single crystal hydrophone to be around -199dBV re 1 µPa.

In Fig. 9, the received level and the calibration curves are shown for the 3 elements summed together, they show a 5dB increase due to array gain, and hence a sensitivity of -194dBV re 1 µPa.

In Fig. 10, the top graph shows the power spectrum densities of the received signal on the reference and each channel of the single crystal hydrophone with pre-amp. Again the single crystal hydrophone follows the shape of the reference fairly well. The bottom graph shows the calibration curves of the signal crystal hydrophone with pre-amp. We can see that single crystal hydrophone is 35 to 40 dB better than the reference. Given that sensitivity of the CT10 is -211dBV re 1µPa, we can estimate the sensitivity of each element of the single crystal hydrophone to be –176 to -171dBV re 1µPa. This close to estimated value of based on the sensitivity of the elements of the single crystal hydrophone without pre-amp, given that the pre-amps have a 25dB gain.

In Fig. 11, the received level and the calibration curves are shown for the 3 elements summed together, they show a 5dB increase due to array gain, and hence a sensitivity of -169dBV re 1µPa.

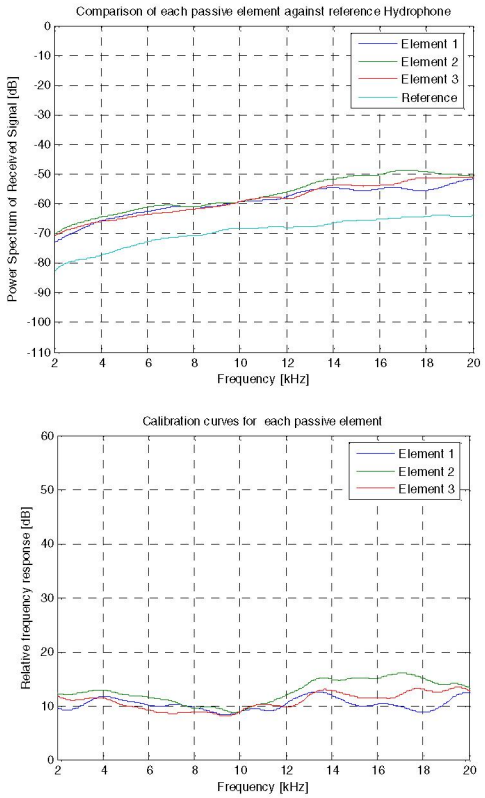

Fig. 8: Power spectrum of received signal and calibration against reference for each element of hydrophone without pre-amp.

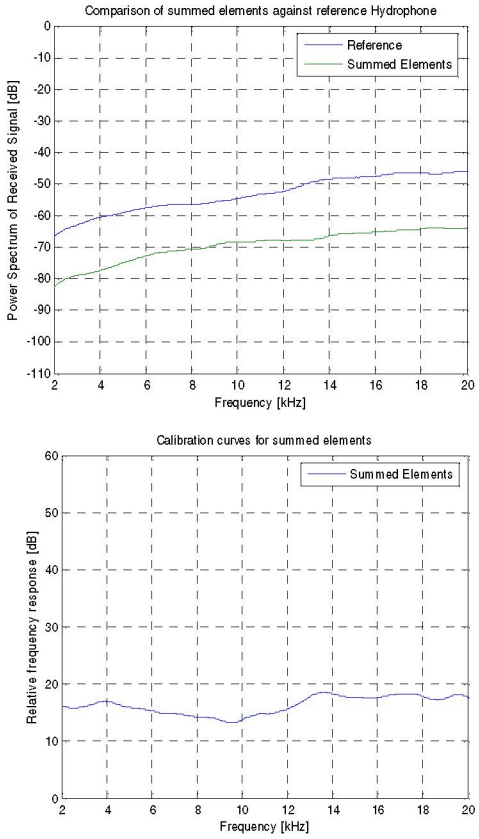

Fig. 9: Power spectrum of received signal and calibration against reference for the summed elements of hydrophone without pre-amp.

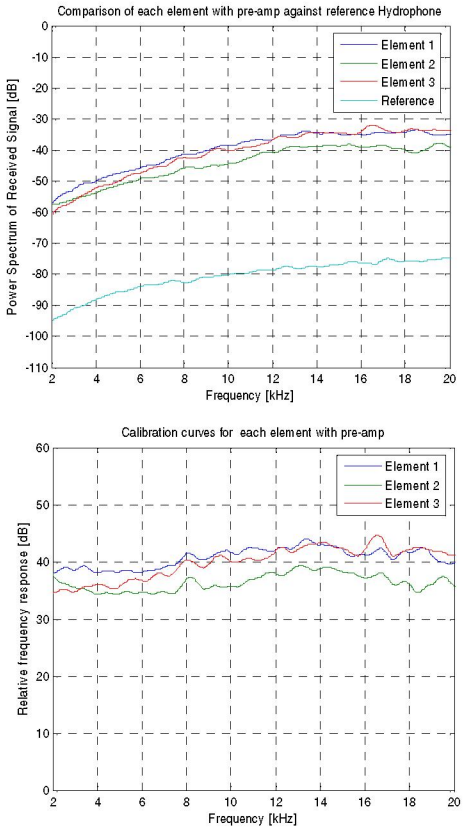

Fig. 10: Power spectrum of received signal and calibration against reference for each element of hydrophone with pre-amp

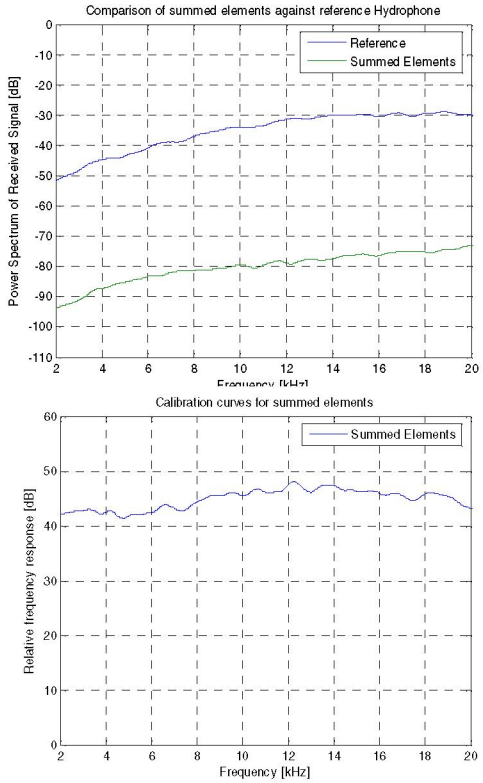

Fig. 11: Power spectrum of received signal and calibration against reference for summed elements of hydrophone with pre-amp.

C. Directionality

In order to measure the directionality, a source transducer is used to emit a single frequency pulse, which is received on the single crystal hydrophone. The hydrophone is then rotated thought a series of angles and the received power is plotted as a function of angle. The source transducer is mounted in a parabolic dish, which helps to produce a more focused beam, this in turn helps to keep down the number of reflections from the water surface and sides of the tank. The received signal on each sensor is cross correlated with the sent signal, and the direct arrival is identified and windowed. A number of pulses are sent and the received direct arrivals are then averaged before the power is calculated and stored. The single crystal hydrophone is rotated in 10 degree increments, and the measurement repeated. To determine the experimental error of this method, the measurements were taken without rotating the single crystal hydrophone, and the variation was found to be less than 0.1 dB.

Figure 12, shows the directionality at 4 and 8 kHz, for each element. The directionality of the individual elements show similar responses, with around ±2dB of variation with direction, and bias in the sensitivity in direction of the element is facing.

Figure 13, shows the directionality at 4 and 8 kHz, for the summed elements. The variation with direction is around ±1dB.

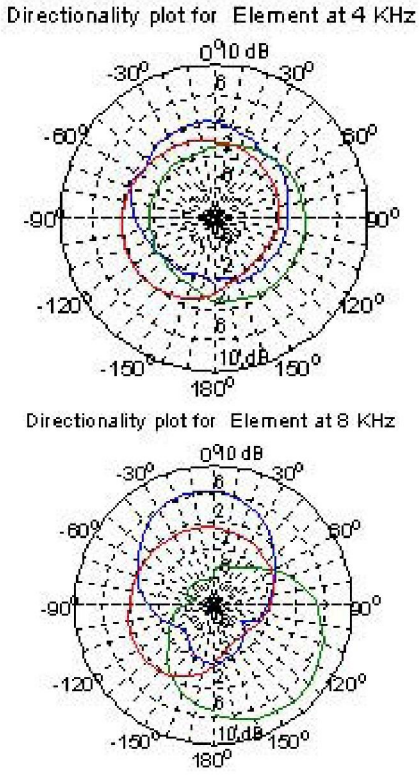

Fig. 12: Directionality of individual elements of the single crystal hydrophone with pre-amp

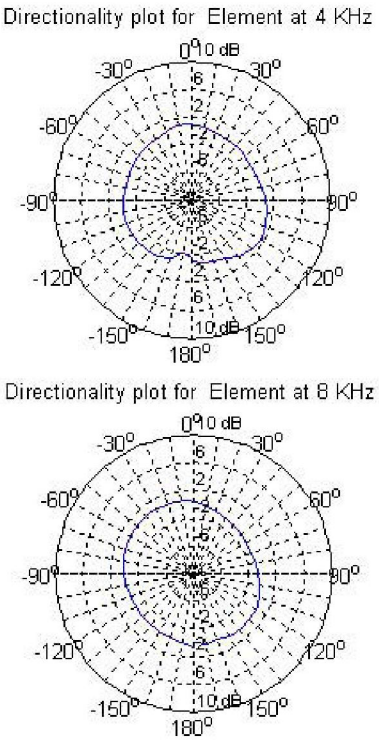

Fig. 13: Directionality for the summed elements of the passive single crystal hydrophone with pre-amp

IV. SUMMARY AND CONCLUSION

A single crystal hydrophone has been developed and tested, by Materials Technologies P/L and ARL. The sensitivity is -169dB re 1 V/µPa. The directionality is fair, being close to omni-directional within ±1dB.

We expect slightly better performance in subsequent iterations, during the development of the upgrades of the preamps and due to improvement in the potting/molding techniques.

REFERENCES

[1] C.D. Motchenbacher and J.A. Connelly, “Low-Noise Electronic System Design”, John Wiley & Sons Inc., USA 1993.

[2] W. Kester, S. Wurcer, and C. Kitchin, “High Impedance Sensors”, Analog Devices, Massechusetts, USA.

[3] Lewis Smith and D.H. Sheingold, “Noise and operational amplifier circuits” Analog Dialogue 25th Anniversary Issue, Analog Devices, Massechusetts, USA, 1999.